Modelling earthquake rupture dynamics across diffuse deforming fault zones

J. Nicolas Hayek (jhayek@geophysik.uni-muenchen.de)[1], Duo Li (dli@geophysik.uni-muenchen.de)[1], Dave A. May[2] & Alice-Agnes Gabriel[1]

[1] Ludwig-Maximilians-Universität (LMU) München, Earth and Environmental Sciences, Germany
[2] University of Oxford, Department of Earth Sciences, United Kingdom

European Research Council
Established by the European Commission

www.tear-erc.eu

1. Introduction

Complex volumetric failure patterns are observed from well-recorded large and small earthquakes [1,2] as well as in laboratory experiments [4]. To understand the mechanics of slip in extended fault zones, the TEAR project (https://www.tear-erc.eu) aims to model **how faults slip** based on the conservation of mass, momentum, and energy using rheological models of **generalized visco-elasto-plastic materials**. We here explore two diffuse fault zone approaches extending the modeling of dynamic earthquake rupture beyond treatment as a discontinuity in the framework of linear elastodynamics:

(i) a **PETSc** [15] **spectral element adaptation of the stress-glut method** [3]

(ii) the **GPR unified first order hyperbolic formulation of hyperelasticity for continuum mechanics** [7, 8, 9] extended for dynamic rupture using a high order Discontinuous Galerkin scheme and the **ExaHyPE** PDE engine [5].

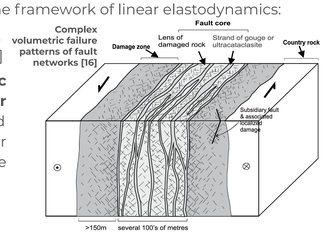

2. Reference Problem

With both methods, we solve the reference problem of a self-similar shear crack problem [10, 12]. The 2D problem [12] consists of a homogeneous and isotropic elastic medium, a linear slip weakening friction law, and the crack propagating along the x axis as depicted in Fig 1. The initial conditions are [10]:

· Density (ρ) = 2500 kg/m^3	· μ_s = 0.5, μ_d = 0.25
· P-wave velocity (V_p) = 4000 m/s	· S-wave velocity (V_s) = 2309 m/s
· Normal stress (S_{yy}) = -40 MPa	· Shear stress (S_{xy}) = 20 MPa
· Characteristic distance (L) = 250 m	· Sliding speed (V) = 2000 m/s

This reference uses an externally imposed traction, and while it does not include the fully dynamic behaviour, it allows to verify the relation between slip, slip rate and traction [10]. We perform numerical refinement analysis based on fault receivers located at 0, 2, 4, 6, 8 km along-strike and a set of receivers perpendicular to the fault at 0, 50, 150, 200, 220m.

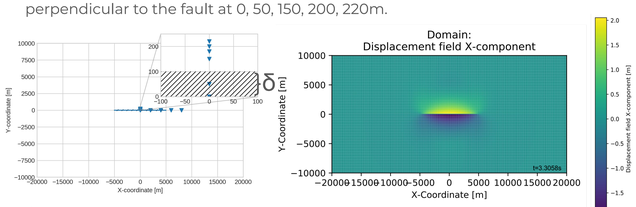

Fig 1. (Left) Fault geometry, model domain, receiver locations (along and perpendicular the fault), and fuzzy fault zone in a signed distance function (SDF) representation. (Right) x component of the displacement from our FE stress-glut method.

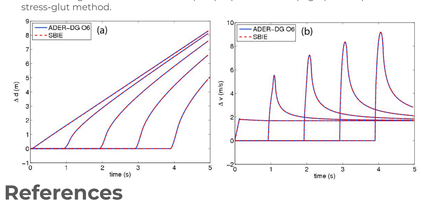

Fig 2. Reference solution from [10] for (a) slip and (b) slip rate.

3. A Spectral Element Stress Glut Approach

3.1 Method

The stress glut (SG) method was originally developed for the finite difference method [13, 14]. There, the SG approximates the fault-jump conditions through inelastic increments to the stress components in a one grid step width inelastic zone. Here we extend the SG method to spectral elements (SESG) using PETSc [15]. The fault zone is represented using a signed distance function (Fig. 1) SESG has the potential to allow for arbitrary fault orientation with respect to the mesh. This includes the use of non-planar faults and time dependent fault geometries. Our method exploits the fact that the stress can be defined locally within each element using local (element-wise) defined quantities.

3.2 Fault representation

The signed distance function (SDF) represents the fault zone independently of the mesh discretization and provides a straightforward manner to compute the normal of the fault. The extended fault is defined by all coordinates for which the absolute value of SDF is <= δ. Thus, the fault thickness is given by 2δ.

3.3 Refinement Study

The spectral element method allows us to refine the spatial resolution of the mesh (h) and the polynomial degree (p) of the basis functions. Additional to this, we can refine the inelastic fault zone thickness (δ). Our stress glut implementation conditions the stress to the critical value of elastic stress yielding inside the inelastic zone. Then, the residual strain is translated into slip rates on the velocity plane, located on the outer limits of the inelastic fault zone.

Depending on the reference solution that we want to compare against, we can vary h, p, δ as refinement parameters.

h- and δ- Refinement

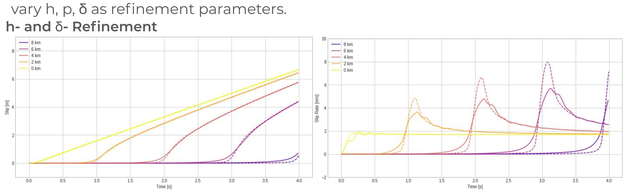

Fig 3 Slip (left) and slip rate (right) for different cell sizes (h) and fault thickness (δ). Solid lines: h = 200 m, δ = 100 m. Dashed lines: h = 50 m, δ = 25m. All simulations used p = 1.

p- Refinement

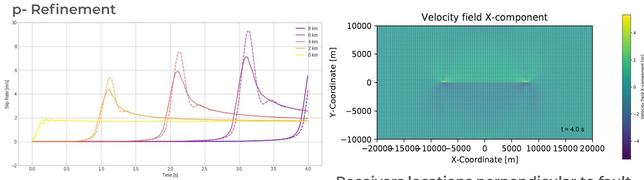

Fig 4. (left) Slip rate under p refinement. Solid lines: h = 100 m, p = 1, δ = 50 m. Dashed lines: h = 100 m, p = 2, δ =50 m. With the latter conditions, we plot the x component of the velocity field from our FE stress-glut method (right).

Receivers locations perpendicular to fault orientation

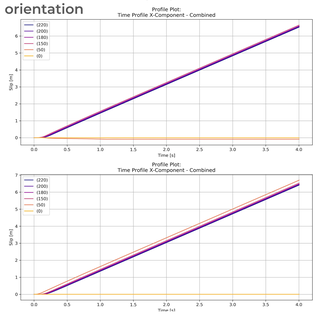

Fig 5. Slip profiles across the fault. Element size (h) = 100 m, p = 2 with δ =100 m (top) and δ = 50 m (bottom). Here, the receivers are located at 0, 50, 150, 200, 220m, perpendicular to the fault. The slip values for the receiver at 50 m become comparable with near off-fault receivers after reducing the inelastic fault thickness to 50 m.

4. Nonlinear hyperelasticity for dynamic rupture in nonlinear elasto-plastic material with a high order accurate discontinuous Galerkin (DG) method

4.1 The Godunov-Peshkov-Romenski (GPR) framework

Instead of an infinitesimal thin fault interface, we model a diffuse fault zone embedded in a continuum visco-plasto-elastic material. We use a unified first order hyperbolic formulation of continuum mechanics, the GPR model [7, 8], which obeys the first and second law of thermodynamics. The GPR model is an extension of nonlinear hyperelasticity, which is able to describe simultaneously nonlinear elasto-plastic solids at large strain, as well as viscous and ideal fluids. The GPR model can account for nonlinear dynamic rupture via an additional scalar describing material damage governed by an advection-reaction equation [9]. We here adopt this method for laboratory derived friction laws of compressional shear cracks in fault zones.

We solve the hyperbolic PDE system using the high performance computing (HPC) toolkit ExaHyPE (https://exahype.eu/), which employs the Arbitrary derivative (ADER) high order discontinuous Galerkin (DG) finite element method [5]. To achieve numerical stability, the numerical scheme employs an a-posteriori sub-cell finite volume limiter on space time adaptive Cartesian meshes [9, 11].

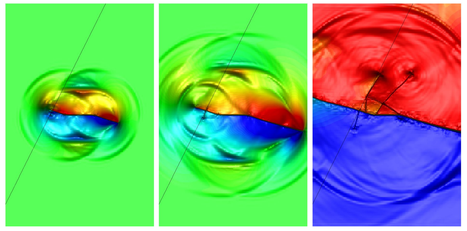

Fig. 6. Evolution of spontaneously growing dynamic rupture and secondary off-plane rupture in a heterogeneous material at 0.5, 0.9, 5.0 sec simulated using the GPR model [Fig. 15 of reference 9]. Here, a von Mises yielding criterion is applied for the off-fault plastic damage. The two types of materials (separated by the black line) are characterized by the critical stress of 180 MPa and 240 MPa, respectively. Supershear rupture can be observed around at the crack front tip. .

GPR formalism:

1) Conservation of mass, momentum and energy:

$$\frac{\partial \alpha}{\partial t} + v_k \cdot \frac{\partial \alpha}{\partial x_k} = 0 \qquad (1)$$

$$\frac{\partial \rho}{\partial t} + \frac{\partial (\rho v_k)}{\partial x_k} = 0 \qquad (2)$$

$$\frac{\partial (\alpha \rho v_i v_j)}{\partial t} + \frac{\partial (\alpha \rho v_i v_j + \alpha p \delta_{ik} - \alpha \sigma_{ik})}{\partial x_k} = 0 \qquad (3)$$

$$\frac{\partial A_{ik}}{\partial t} + \frac{\partial A_{im} v_m}{\partial x_k} + v_m \left(\frac{\partial A_{ik}}{\partial x_m} - \frac{\partial A_{im}}{\partial x_k} \right) = -\frac{1}{\theta_1(\tau_1)} E_{A_{ik}} \qquad (4)$$

$$\frac{\partial J_k}{\partial t} + \frac{\partial (J_m v_m + T)}{\partial x_k} + v_m \left(\frac{\partial J_k}{\partial x_m} - \frac{\partial J_m}{\partial x_k} \right) = -\frac{1}{\theta_2(\tau_2)} E_{J_k} \qquad (5)$$

$$\frac{\partial \xi}{\partial t} + v_k \cdot \frac{\partial \xi}{\partial x_k} = -\theta E_\xi \qquad (6)$$

$$\frac{\partial \rho S}{\partial t} + \frac{\partial (\rho v_k S + \rho E_{J_k})}{\partial x_k} = \frac{\rho}{T} \left(\frac{1}{\theta_1} E_{A_{ik}} E_{A_{ik}} + \frac{1}{\theta_2} E_{J_k} E_{J_k} + \theta E_\xi E_\xi \right) \geq 0 \qquad (7)$$

$$\frac{\partial (\rho E)}{\partial t} + \frac{\partial (v_k \rho E + v_i (p \delta_{ik} - \sigma_{ik}))}{\partial x_k} = 0 \qquad (8)$$

α is the diffuse interface coefficient, v_i is velocity, ρ is density, p is hydrostatic pressure, σ_{ik} is total stress tensor; A_{ik} is distortion field, J_k is thermal impulse, T is temperate, S is the entropy, θ is a function of the state parameters determining the rate of damage, ξ is damage coefficient, the total energy potential $E = E(\rho, S, v, A, J, \xi)$, τ_1 and τ_2 is shear or thermal relaxation time.

2) Constitutive laws:

$$\sigma'_{ij} = \sigma'_{ij} + p\delta_{ij} \qquad (9)$$

$$\sigma'_{ij} = \rho A_{jk} E_{A_{ik}} + \rho J_i E_{J_k} \qquad (10)$$

$$P = \rho^2 E_\rho \qquad (11)$$

σ'_{ij} is total stress tensor; σ'_{ij} is deviator stress tensor; P isotropic pressure.

3) Damage evolution:

$$\tau_1 = \frac{1}{(1-\xi)\tau_2 + \xi \tau_D} \qquad (12)$$

$$\tau_D = \tau_{D0} \exp(\alpha_1 - \beta_1 (1-\xi) Y) \qquad (13)$$

$$\tau_2 = \tau_{D0} \exp(\alpha_2 - \beta_2 \xi Y) \qquad (14)$$

$$\theta = (1-\xi)\xi + \xi_c |(1-\xi)(\frac{Y}{Y_c})^p + \xi(\frac{Y}{Y_f})| \qquad (15)$$

τ_D and τ_2 is shear relaxation time for damaged and intact materials. $\tau_{D0}, \tau_{D0}, \alpha_1, \beta_1, \alpha_2, \beta_2$ are constant parameters for various rock materials. Y is critical stress from von Mises criterion. a, Y_0, Y_f are constants.

(Details can be found in Tavelli, et al., 2020 arXiv:2003.02760)

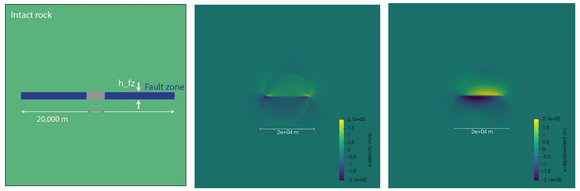

Fig. 7. (Left) Sketch of the fault zone setup (not to scale). The initial condition and material properties are stated in Sec. 2. (Middle) Velocity field (x-component) at 4 sec in the rupture model. Length scale is 20,000 m. The width of the diffuse fault zone is h_fz=213 m. (Right) Displacement field (x-component) at 4 sec. The emanated wave field is shown as horizontal particle velocity.

4.3 Refinement analysis

➢ **p-refinement: order 3 vs. order 6**

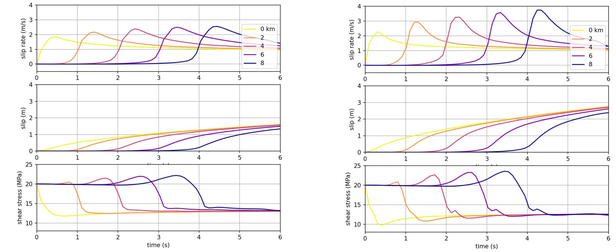

Fig. 8. On-fault results of a self-similar crack model. Each line represents an on-fault station at a certain distance away from the fault center. Fault zone width is 200 m. Spatial resolution is 933 m and polynomial order 3 (left) and order 6 (right). The equivalent FV sub-cell sizes are ~213 and ~71 m, respectively. Slip rate, slip and stress drop will increase with polynomial order when the fault zone width is constant.

➢ **Fault zone width decrease: 213 m vs. 71 m**

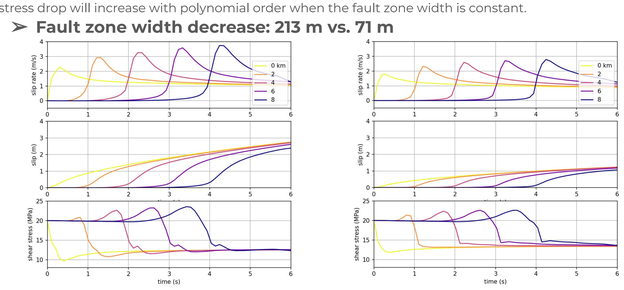

Fig 9. The spatial resolution is the same while fault zone width is 213 m (left) and 71 m (right). On-fault stations are the same as Fig. 8. Spatial resolution is 933 m and polynomial order 6 (the equivalent FV sub-cell size is 71 m). Slip rate, slip and stress drop will decrease with fault zone when polynomial order is constant.

5. Summary and Outlook

➢ We extend the classical **stress glut** method to **spectral elements**. The implementation aims to permit modeling of **non-planar faults and time-dependent fault geometries.**

➢ **Refinement analysis** for a self-similar crack problem shows slip and slip rate approaching the reference solution when increasing polynomial order, or decreasing mesh size and fault zone thickness simultaneously.

➢ Shrinking the thickness of the fault zone implies formation of a discontinuity in slip and slip rate, as in classical dynamic rupture modeling.

➢ We extend the **GPR model of continuum mechanics** with **an additional dynamic process that describes material failure** during dynamic earthquake rupture. Damage is governed by an advection-reaction equation, and the reaction source term can resemble friction laws.

➢ Refinement analysis for a self-similar crack problem shows, that on-fault slip rate and slip increase with polynomial order when the fault zone width is kept constant. Slip rate and slip will decrease with fault zone width when polynomial order is constant.

➢ On-fault slip rate as well as wavefields of both methods are comparable to the reference.

➢ We will next extended both methods to full dynamic rupture benchmarks, specifically including off-fault plasticity.

References

1. Y. Cheng, Z.E. Ross, and Y. Ben-Zion. Diverse volumetric faulting patterns in the San Jacinto fault zone. *JGR: Solid Earth*, 123(6):5068-5081, 2018.
2. Y. Klinger, K. Okubo, A. Vallage, J. Champenois, A. Delorme, E. Rougier, Z. Lei, E.E. Knight, A. Munjiza, C. Satriano, et al. Earthquake damage patterns resolve complex rupture processes. *GRL*, 45(19):10-279, 2018.
3. R. Madariaga, K. Olsen, and R. Archuleta. Modeling dynamic rupture in 3D earthquake fault model. *BSSA*, 88(5):1182-1197, 1998.
4. F.X. Passelègue, E. Spagnuolo, M.Violay, S. Nielsen, G. di Toro, and A. Schubnel. Frictional evolution, acoustic emissions activity, and off-fault damage in simulated faults sheared at seismic slip rates. *JGR: Solid Earth*, 121(10):7490-7513, 2016.
5. A. Reinarz, D.E. Charrie, M. Bade, L. Bovard, M. Dumbser, K. Duru, F. Fambri, A.-A. Gabriel, J.-M. Gallard, S. Köppel, et al. Exahype: an engine for parallel dynamically adaptive simulations of wave problems. *arXiv preprint arXiv:1905.07987*, 2019.
6. I. Van Zelst, S. Wollherr, A.-A. Gabriel, E.H. Madden, and Y. van Dinther. Modeling megathrust earthquakes across scales: One-way coupling from geodynamics and seismic cycles to dynamic rupture. *JGR: Solid Earth*, 124(11):11414-11446, 2019.
7. S.K. Godunov and E.I. Romenski. Nonstationary equations of nonlinear elasticity theory in eulerian coordinates. *J Appl. Mech. Tech. Phys.*, 13(6):868{884, 1972
8. I. Peshkov and E. Romenski. A hyperbolic model for viscous newtonian flows. Continuum Mechanics and Thermodynamics, 28:85{104, 2016
9. M. Tavelli, S. Chiocchetti, E. Romenski, A.-A. Gabriel, M. Dumbser, Space-time adaptive ADER discontinuous Galerkin schemes for nonlinear hyperelasticity with material failure. arXiv:2003.02760, doi:arXiv:2003.02760, submitted.
10. de la Puente, J., J.-P. Ampuero and M. Käser. Dynamic rupture modeling on unstructured meshes using a discontinuous Galerkin method. *JGR: Solid Earth*, 114(B10), 2009
11. Dumbser, M., I. Peshkov, E. Romenski and O. Zanotti. High order ADER schemes for a unified first order hyperbolic formulation of continuum mechanics: Viscous heat-conducting fluids and elastic solids. *JCP*, 314: 824-862, 2016
12. Kostrov, B. V. Self similar problems of propagation of shear cracks. *J. Appl. Math. & Mech.*, 28(5), 1077-1087, 1964.
13. Andrews, D. J. Rupture velocity of plane strain shear cracks. *JGR*, 81(32), 5679-5687, 1976.
14. Dalguer, L. A., and Day, S. M. Comparison of fault representation methods in finite difference simulations of dynamic rupture. *BSSA*, 96(5), 1764-1778, 2006.
15. Portable Extensible Toolkit for Scientific computation (PETSc) https://www.mcs.anl.gov/petsc
16. Mitchell, T. M., & Faulkner, D. R. (2009). The nature and origin of off-fault damage surrounding strike-slip fault zones with a wide range of displacements: A field study from the Atacama fault system, northern Chile. Journal of Structural Geology, 31(8), 802-816.